

# Observing Dynamic State of River-Mouth Bar and its Control in the Yuragawa River

H. Miwa

*National Institute of Technology, Maizuru College, Kyoto, Japan*

K. Kanda & T. Ochi

*National Institute of Technology, Akashi College, Hyogo, Japan*

K. Yamasaki

*NTT Infrastructure Network Corporation, Osaka, Japan*

H. Murakami

*Kyoto University, Kyoto, Japan*

**ABSTRACT:** Topographic changes of the river-mouth bar in the Yuragawa River are continuously activated by river and ocean currents and sea wave. The bar recently has the imbalance situation of its geometry, it may cause sedimentation problems. In order to avoid the problems, it is important to understand the characteristics of the topographic change of the river-mouth bar, and to propose a control method of the bar geometry. In this study, variations in geometrical properties of the river-mouth bar are analyzed on the basis of the hydrological data (river water discharge and sea wave height). As for the bar control, the effectiveness of spur dikes, which can change the flow direction, for erosion of the bar was evaluated by means of flume experiments. The two-dimensional numerical model (iRIC Project) is also applied to further investigate the effect of spur dike on the bar control. Through this study, we clarify the efficiency of sandbar control at the mouth of the river in the Yuragawa River.

*Keywords: Yuragawa River, River-mouth bar, Topographic change, Field observation, Spur dike, Flume experiment, Numerical simulation*

## 1 INTRODUCTION

The Yuragawa River is located in the north of Kyoto Prefecture, the mid-west in Japan, as shown in Fig.1. The origin of the river is Mikunidake situated on the borders of three prefectures of Kyoto, Fukui and Shiga. The length of the river is 146 km, and the size of its basin is 1,880 km<sup>2</sup>. The Yuragawa river system is one of the 109 Class A river systems in Japan. The Yuragawa River can be classified into three reaches. In the upper reaches, V-shaped ravines and river terraces are developed. The width of river increases in the middle reaches and pools and riffles are developed in the main channel of the river. The lower reaches consist of the valley plain, the stream flows along the long and narrow bottom of the mountains. Figure 2 shows the longitudinal bed profile of the lower and middle reaches of the Yuragawa River. The average bed gradient around Fukuchiyama (37 km far from the river-mouth) in the middle reaches is about 1/1,500, whereas the bed gradient in the lower reaches is approximately 1/6,000 to 1/8,000. Therefore, the length of tidal section of the river reaches over 20 km.

Topographic change of river-mouth consists of complicated interactions of river and marine forces. On October 2004, a large part of the river-mouth bar was eroded by the flood flow of the typhoon No.23. After that, the river-mouth bar has developed on the right bank only, and the river-mouth channel has been fixed along the left bank. This situation may cause some problems such as bank erosion, washout of bank protection works and harmful effects on other coastal structures. Effects of water discharge during flood periods on responses of the river-mouth bar are also not clarified. Therefore, the risk of high water level caused by a river-mouth clogging is high. In order to avoid these problems and risk, it is important to understand the characteristics of the topographic change of the river-mouth bar and its cause, and to propose a control method of the bar geometry.

In this study, the temporal variations in geometrical properties (e.g., bar area and shape) of the river-mouth bar were analyzed on the basis of the hydrological and topographical data in the Yuragawa River

estuary. The effects of the river water discharge and the sea wave height on the geometrical properties of the bar were also investigated. In order to investigate responses of area, height and volume of the bar against flood discharges, two-dimensional numerical analysis was conducted next. As for the bar control, the effectiveness of a spur dike, which can change the flow direction, for erosion of the bar was evaluated by means of flume experiments. The two-dimensional numerical model was also applied to further investigate the effects of spur dike on the bar control. The simulation results were verified against the experimental results.



Figure 1. Location and basin of Yuragawa River.

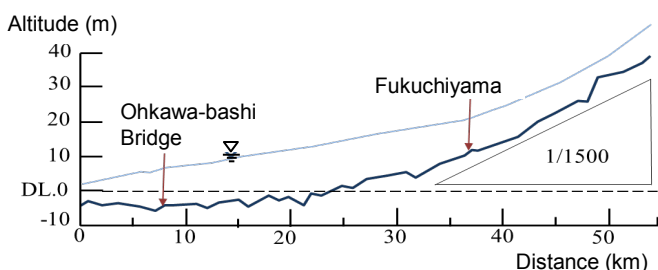


Figure 2. Longitudinal bed profile of lower and middle reaches.

## 2 FIELD MEASUREMENT ON DYNAMIC STATE OF RIVER MOUTH TOPOGRAPHY

### 2.1 Changes of river-mouth topography for 60 years

Figure 3 shows the changes of river-mouth topography from 1947 to 2009. In 1947 and 1963, the river-mouth bar on the right bank was developed considerably and the width of the river-mouth channel was approximately 80-100 m. The river-mouth bar on the right bank was disappeared and it on the left bank was developed in 1972. The river-mouths on the both bank were developed in 1975 and 1982. The widths of the river-mouth channel were approximately 80 m for both years. After that, a large part of the river-mouth bar was flushed out by the flood flow (peak discharge  $Q_p=3,600 \text{ m}^3/\text{s}$ ) of the typhoon No.10 in 1982 and 1983, the width of the river mouth channel increased to about 300 m. However, the river-mouth bars were developed as shown in photographs of 1986 to 2001. A large part of the river-mouth bar was flushed out again by the flood flow (peak discharge  $Q_p=5,400 \text{ m}^3/\text{s}$ ) of the typhoon No.23 in 2004. The river-mouth bar has developed on the right bank only after then, and the river-mouth channel has been fixed along the left bank (2009).

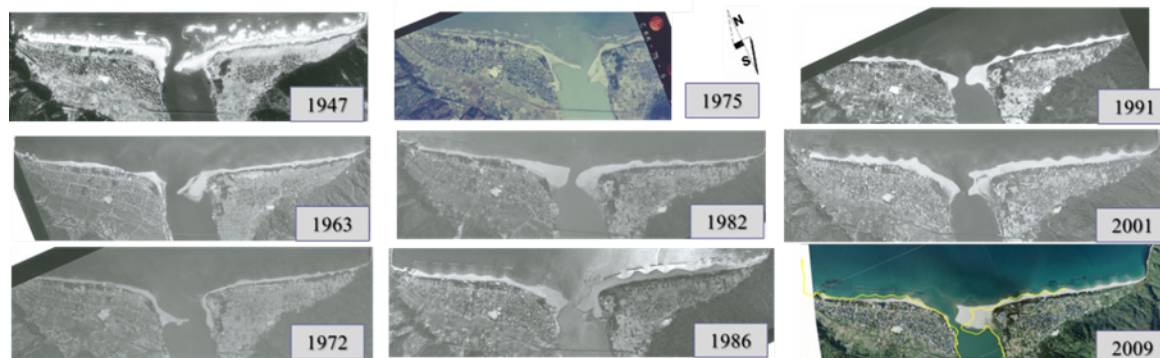


Figure 3. Temporal changes of river-mouth topography in Yuragawa River (1947-2009).

The construction works of detached breakwaters have been carried out from 1967 and there are 8 detached breakwaters for each bank. The formation of tombolo is confirmed after 1982. Effects of the detached breakwaters on river-mouth bar formation are not clarified.

## 2.2 Results of fields measurement

In order to clarify the effects of river flow discharge and sea wave height on change of river-mouth topography, Topographical survey works of the river-mouth topography have been conducted by using GPS periodically. A surveyor walked along the shore line receiving the satellite signals, and registered the signal to the controller at intervals of approximately 10 to 20 m. The number of stations for each survey was about 70 to 100. The area of the bar and its shape were calculated by means of the coordinates of the stations. Basically, the survey was conducted once a month.

Figure 4 shows the temporal variations in the area of the river-mouth bar for four years (from May 2010 to April 2014). The datum level was the sea surface at each measurement time, and there was no correction of the datum level because the tidal range was at most 30 cm. The river-mouth bar on the left bank has developed from December 2012 (The survey was started in March 2013). In the Fig.4, the area of the bar on right bank shows increase and decrease in the short term, whereas it gradually decreases as a long term tendency. The decreasing rate of the area for four years is approximately 40 %. From the short term tendency, it can be found that the area was increased in the winter season of 2010, 2012 and 2013, and it was decreased in the rainy and summer season of 2011 and 2013. The time series of the significant wave height at Kyoga-Misaki (30 km far from the river-mouth) for the same period as the area of the bar is shown in Fig.5. Kanda et al. (2012) clarified the significant wave height over 2.55 m influences the development of the river-mouth bar. Therefore, it can be considered that an increase of the onshore sediment transport may contribute the increase of the area of the river-mouth bar. The reason why the area did not increase in the winter season of 2011 is the onshore transported sediment from the foreshore may be accumulated on the seabed, where it was eroded by the flood flow in the fall season of 2011. The time series of the water discharge at Fukuchiyama for the same period as the area of the bar is shown in Fig.6. The water discharge over 1,500 m<sup>3</sup>/s has been recorded totally four times in the summer season of 2011 and 2013. In particular, the flood with discharge of about 5,500 m<sup>3</sup>/s occurred due to the typhoon No.18 in September 2013. The area of the bar was reduced of 17% in 2011 and of 40% in 2013 by these large flood discharges. Moreover, it is found that the area was gradually reduced in the spring to fall seasons of 2012. The water discharge of 300 m<sup>3</sup>/s classes had frequently occurred during these seasons, these flows might have eroded the river-mouth bar.

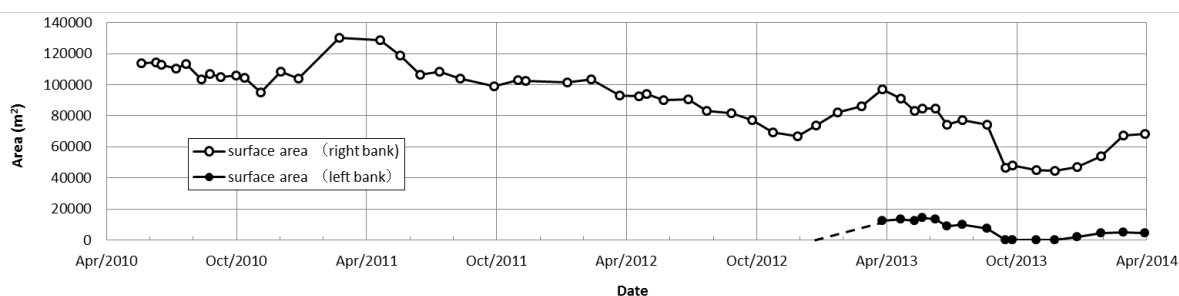


Figure 4. Temporal variations in area of river-mouth bar in Yuragawa River.

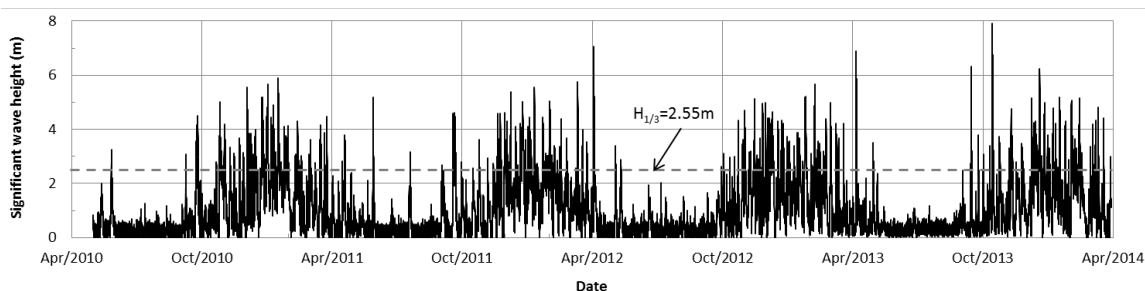


Figure 5. Temporal variations in significant wave height at Kyoga-Misaki.

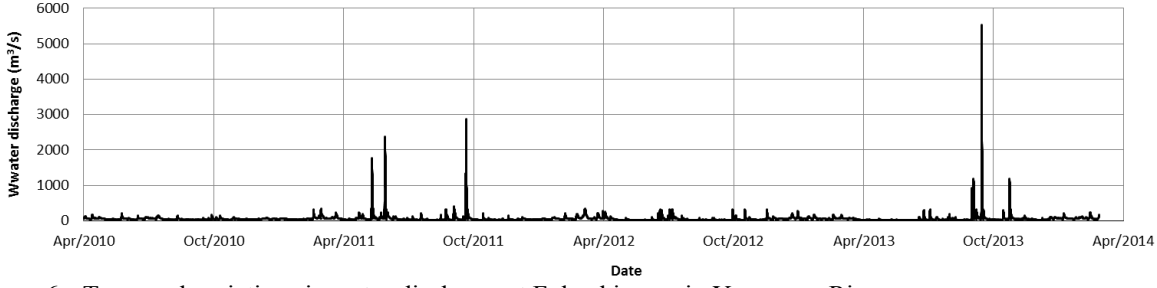


Figure 6. Temporal variations in water discharge at Fukuchiyama in Yuragawa River.

### 3 EFFECTS OF SIZE OF FLOOD DISCHARGE ON EROSION OF RIVER-MOUTH BAR IN YURAGAWA RIVER

#### 3.1 Simulation model and its governing equations

Since morphological changes of the river-mouth bar depend not only on the significant wave heights and water discharges but also the topography of its surrounding region, it is important to deal with large area including the river-mouth bar. We investigate here the effects of the size of flood discharge on the river-mouth topography by means of the numerical simulation model.

The simulation model Nays2D (iRIC, 2013) was applied to the investigation in this study. The continuity equation and the momentum equations are

$$\frac{\partial h}{\partial t} + \frac{\partial(uh)}{\partial x} + \frac{\partial(vh)}{\partial y} = 0 \quad (1)$$

$$\frac{\partial(uh)}{\partial t} + \frac{\partial(hu^2)}{\partial x} + \frac{\partial(huv)}{\partial y} = -hg \frac{\partial H}{\partial x} - \frac{\tau_x}{\rho} + D_x \quad (2)$$

$$\frac{\partial(vh)}{\partial t} + \frac{\partial(huv)}{\partial x} + \frac{\partial(hv^2)}{\partial y} = -hg \frac{\partial H}{\partial y} - \frac{\tau_y}{\rho} + D_y \quad (3)$$

where  $x, y$  = plane Cartesian coordinates,  $u, v$  = velocity components in  $x$  and  $y$  direction,  $t$  = time,  $h$  = water depth,  $H$  = water elevation,  $g$  = gravity acceleration,  $\rho$  = fluid density,  $\tau_x, \tau_y$  = bed shear stress components in  $x$  and  $y$  direction,  $D_x, D_y$  = diffusion term in  $x$  and  $y$  direction, respectively.

Uniform sediment bed is assumed in this study. The continuity equation of sediment transport is

$$\frac{\partial z}{\partial t} + \frac{1}{1-\lambda} \left( \frac{\partial q_{bx}}{\partial x} + \frac{\partial q_{by}}{\partial y} + q_{su} + w_f c_b \right) = \frac{q_B}{1-\lambda} \sqrt{\frac{\tau_{*c}}{\mu_s \mu_k \tau_*}} \left( \frac{\partial^2 z}{\partial x^2} + \frac{\partial^2 z}{\partial y^2} \right) \quad (4)$$

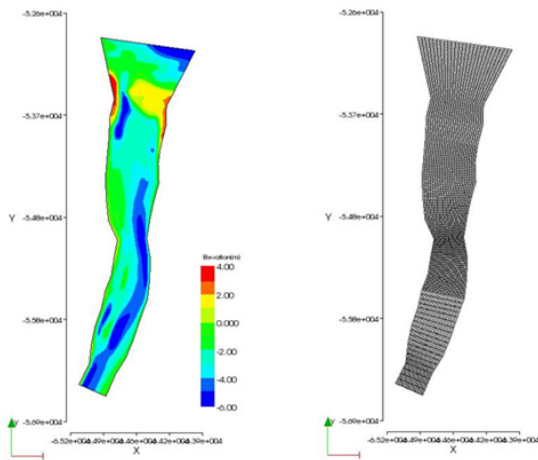
where  $z$  = bed elevation,  $\lambda$  = bed porosity,  $q_{bx}, q_{by}$  = bed-load sediment transport rates per unit width in  $x$  and  $y$  direction,  $q_{su}$  = release rate of sediment from bed,  $w_f$  = settling velocity of sediment,  $c_b$  = reference concentration of suspended sediment,  $q_B$  = bed-load sediment transport rate per unit width in streamline direction,  $\mu_s, \mu_k$  = static and kinetic friction coefficient of bed material,  $\tau_*, \tau_{*c}$  = dimensionless bed shear stress and dimensionless critical bed shear stress, respectively.

The governing equations mentioned above and others are transformed into discrete forms in a generalized coordinate system. In the simulation model, the advection terms are discretized by the CIP method and the zero equation model is applied as a turbulence model. As for the sediment transport equation, the Ashida-Michiue equation (1972) for  $x$  direction and Hasegawa equation (1983) for  $y$  direction are employed in the model.

#### 3.2 Simulation methods and results

The contour line and the computational grid of the calculation area which is based on the bathymetric survey of October 2010 are shown in Fig.7. The longitudinal range of the area is -0.6 kp to 3.0 kp, and the area is divided into 25 grids for lateral direction and into 150 grids for longitudinal direction (the grid intervals of 20 m for -0.6 kp to 2.0 kp and them of 50 m for 2.0 kp to 3.0 kp). The mean grain diameter of

the sediment is set to  $d_m = 0.3$  mm and the Manning's roughness coefficient is taken as  $n = 0.020$ . The water discharge conditions are set to five cases of  $Q = 1,500$  to  $3,500$   $m^3/s$  with intervals of  $500$   $m^3/s$ . The duration time of the water discharge is taken as three hours. The sea level is given as  $h_d = 0.458$  m of the high water level at the Maizuru Marine Observatory. The time increment ( $\Delta t$ ) is taken as  $0.01$  second. In the computation, the water discharge and sea level are given at the upstream and downstream boundaries, respectively.



(a) contour line (b) computation grid

Figure 7. Contour line and computational grid of calculation area in Yuragawa River.

Figure 8 shows temporal variations in area, height and volume of the river-mouth bar.  $A_0$ ,  $H_0$  and  $V_0$  in the vertical axis are the initial value of them, respectively. The bar area begins to decrease at  $Q = 2,000$   $m^3/s$ , and it considerably decreases at over  $Q = 3,000$   $m^3/s$ . The bar height also decreases at over  $Q = 2,000$   $m^3/s$ . The decrease rate reaches steady state at about an hour and it hardly change after that. Therefore, it can be considered that effect of the continuous high water discharge on the bar height is relatively small. Under the situation of decrease of the bar volume for each water discharge condition, the variation in the area shows similar tendency between  $Q = 2,000$  and  $2,500$   $m^3/s$ , and the variation in the height shows similar tendency between  $Q = 2,500$  and  $3,000$   $m^3/s$ . This result may mean that the changing mechanisms of the area and height of the bar on the erosion mechanisms of the mouth-bar are different each other by the amount of the water discharge.

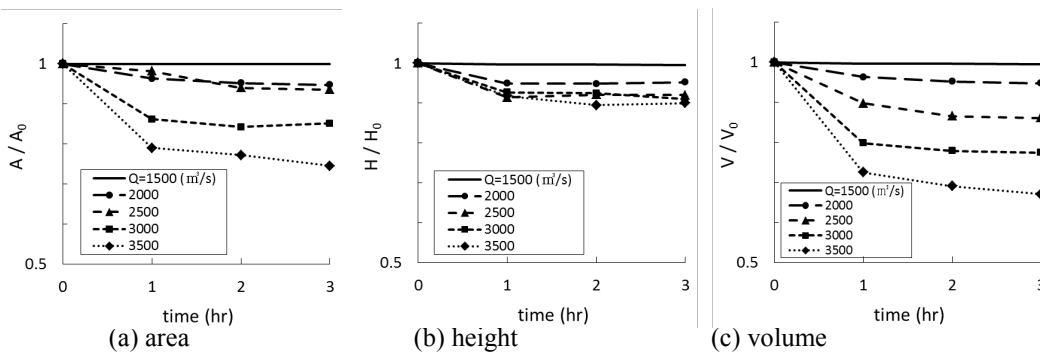


Figure 8. Temporal variations in responses of river-mouth bars to flood discharge.

## 4 RIVER-MOUTH BAR TOPOGRAPHY CHANGE DUE TO FLOOD DISCHARGE AND ITS CONTROL BY SPUR DIKES

### 4.1 Flume experiment

#### 4.1.1 Experimental set-up and procedure

Flume experiments using the large channel, which was modeled based on the Yuragawa River, were conducted in order to clarify effects of spur dikes on control of the river-mouth bar topography. The experiments were conducted in a horizontal rectangular open channel with  $8.75$  m long and  $2.87$  m wide as shown in Fig.9. The width of this channel corresponds with  $1/150$  scale of the Yuragawa River. The channel has a water level adjusting weir in the returning flume in order to control the water elevation at the downstream end of the channel. The nearly uniform coal dust was used in the experiments as the bed

sediment. The coal dust has a mean grain diameter  $d_m$  of 1.3 mm and a specific gravity  $\sigma_s$  of 1.47.

The movable bed was flattened with a scraper and the river mouth-bar model, which was modeled based on the results of topographical survey, was formed on the channel bed (Fig.9.). The river mouth-bar is located on the right bank in the Yuragawa River, but the river-mouth model was set to the left bank in order to avoid the effect of the lateral flow toward the returning flume. The height of the river-mouth bar was 0.02 m, the sea bed behind the river-mouth bar was set to a slope  $I_b$  of 0.05 (1/20). The other part of the bed was made horizontally.

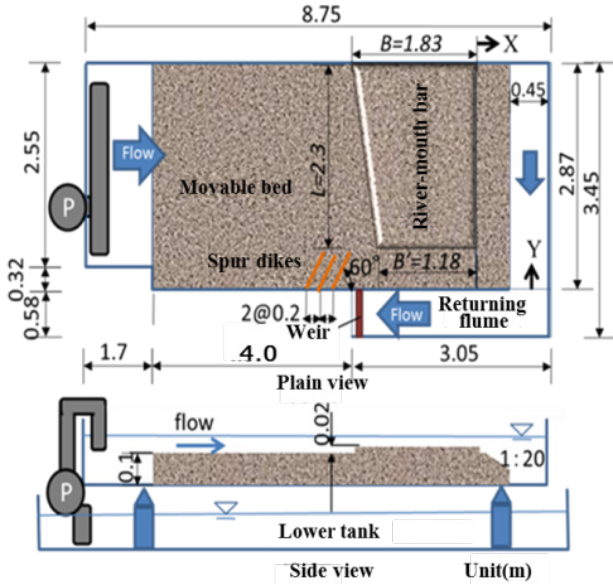


Figure 9. Experimental set-up.

The experimental conditions are listed in Table 1. In the table,  $Q$  = water discharge,  $T$  = duration of experiment,  $h_d$  = water surface elevation at downstream end of the channel,  $L$  = length of spur dike. The discharges in the experiments correspond with the flood discharge of  $Q = 2,800$  to  $3,000 \text{ m}^3/\text{s}$ . The duration of experiment corresponds with the duration of peak discharge of  $T = 3.7$  hours. The spur dike was made of plywood, its thickness and height were 0.01 m and 0.12 m, respectively. Its length was two types of 0.3 m and 0.6 m. Three pieces of spur dike were set on the right bank at intervals of 0.2 cm with angle of 60 degrees as shown in Fig.9.

In the experiment, the water was stored slowly in the channel in order to avoid erosion of the bed. The prescribed water discharge was fed into the channel after that. The water elevation at the downstream end of the channel was controlled by the water level adjusting weir. Water surface elevations were measured with a point gauge, at intervals of 1 m in the longitudinal direction at the location of  $Y = 0.8$  m of the channel before stopping the flow. The motion of PVC particles (particle size =  $50 \mu\text{m}$ ) on the water surface was recorded by using a video camera for 20 second during the experiment. The surface velocity was obtained from PIV analysis (Fujita, 1998). Transverse profiles of the bed surface were measured with a laser sensor mounted on a propelled carriage, at intervals of 4 cm in the longitudinal direction of the channel after stopping the flow. The datum plane for water surface and bed surface elevations was set to the channel-bed surface. Then, initial bed elevation was 0.1 m for the river bed part and was 0.12 m for the river-mouth bar part.

Table 1. Experimental conditions.

Case	$Q$ (l/s)	$T$ (min)	$h_d$ (m)	$L$ (m)
1	10.8	20	0.143	none
2	10.7	20	0.147	0.3
3	10.0	20	0.139	0.6

#### 4.1.2 Experimental results and discussions

Figure 10 illustrates the change of river-mouth bar topography by the spur dikes. The area surrounded by break line shows the initial shape of the river-mouth bar. The surface velocity distributions around the river-mouth bar are also shown in Fig.11. In the case of no spur dikes (Case 1), the flow converges toward the river-mouth on the right bank, and progresses erosion of the river-mouth channel. Although the

flow gets over the river-mouth bar, the erosion of its surface hardly occurs because its velocity is relatively slow. In the case of the short spur dikes (Case 2), the converged flow toward the river-mouth is weakened by setting the spur dikes. And, the front part of the river-mouth bar is eroded more by the redirected flow due to the spur dikes. The erosion of the bar surface hardly occurs in this case too. In the case of the long spur dikes (Case 3), the scour depth of the river-mouth channel becomes small because the spur dikes redirect strongly the flow toward the river-mouth bar. The redirected flow erodes the river-mouth bar in this case. It is found that the sediments deposit at the lower part of the spur dikes because the flow intensity is weak there. The flow gets over river-mouth bar and erodes its surface. From the mentioned above, it is considered that the spur dike work is effective for control of the river-mouth bar.

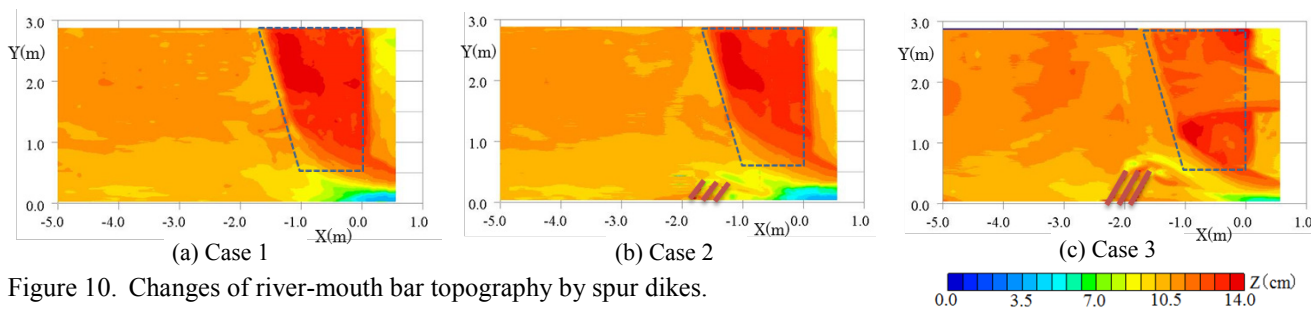


Figure 10. Changes of river-mouth bar topography by spur dikes.

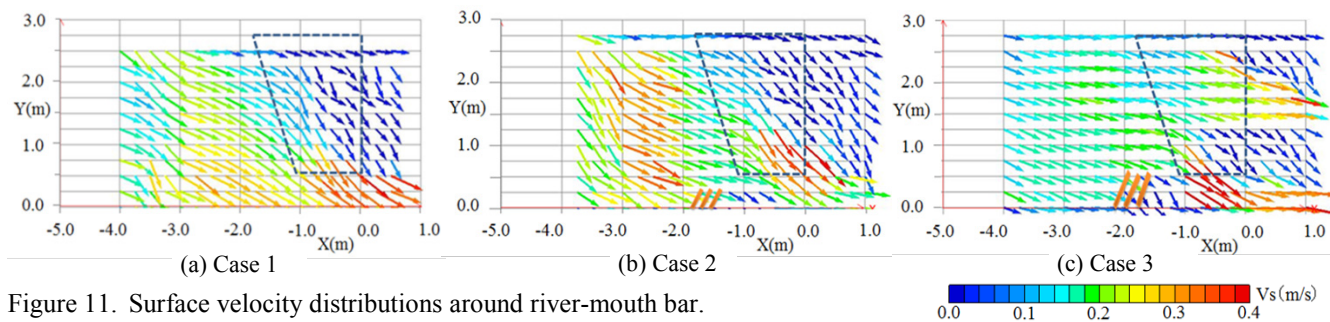


Figure 11. Surface velocity distributions around river-mouth bar.

#### 4.2 Numerical simulation, results and discussions

Numerical simulations were conducted in order to further investigate the control method for the river-mouth bar topography. Nays2D, which is mentioned in Chapter 3, was used in the simulation. Rectangular coordinates are used in the simulation. The channel (5.68 m long, 2.84 m wide) was divided into 142 and 71 grids for the longitudinal and lateral directions, respectively. Then, the longitudinal grid size ( $\Delta x$ ) and the lateral grid size ( $\Delta y$ ) are the same as 0.04 m. The Manning's roughness coefficient and the time increment are taken as  $n = 0.020$  and  $\Delta t = 0.01$  second, respectively. The value of  $h_d$  are set as 0.14, 0.13 and 0.13 m for the Case 1, Case 2 and Case 3, respectively, in order to promote the bed variation. Other parameters and hydraulic conditions are the same as the experiments.

Figure 12 illustrates the reproduction calculation results of the flume experiments. The vectors mean the depth averaged flow velocities. The flow converges toward the river-mouth and the erosion of the river-mouth bar is relatively small in Case 1. The flow around the spur dikes is redirected to the river-mouth bar. Therefore, the front part of the bar is eroded more in Case 2 and the width of the river-mouth channel becomes large. In Case 3, the erosion of the river-mouth bar is more active, transported sediments are accumulated behind the bar like a sand spit. The scour of the river-mouth bar channel is restrained because the width of the channel becomes large. Although the flow gets over the river-mouth bar, the bar surface are hardly eroded in all cases. These simulation results can reproduce the most of the experimental results. However, the erosion of the bar surface in Case 3 cannot be reproduced in the simulation. This problem may be caused by the boundary condition at the downstream end of the channel.

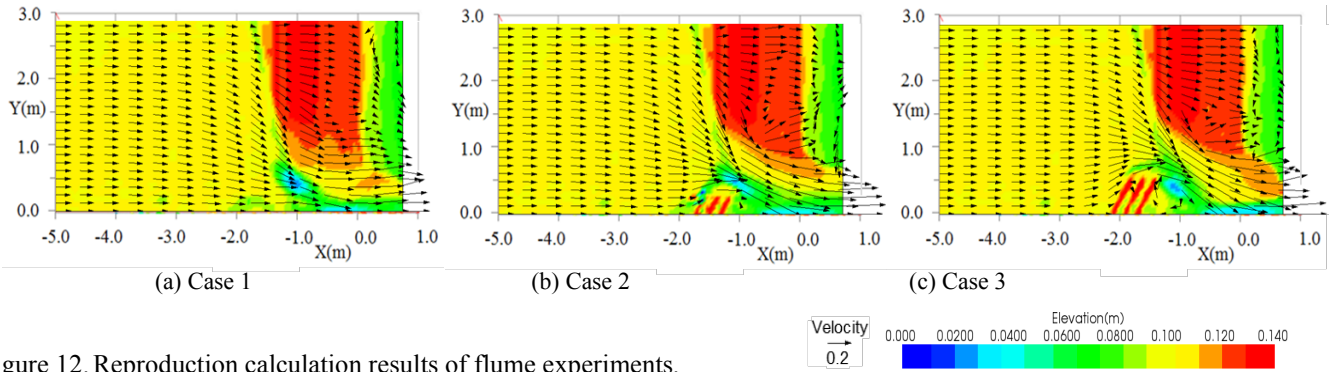


Figure 12. Reproduction calculation results of flume experiments.

## 5 CONCLUSIONS

The results obtained in this study are summarized as follows:

- (1) Although the bar area and volume of the river-mouth bar showed the short-term fluctuations due to flood, they also showed the increase tendency on a long-term basis. The flush condition of the river-mouth bar sediments due to flood does not depend on the width of river-mouth channel and the bar area but on flood discharge. The formation of river-mouth bar may be mainly activated by an increase of longshore sediment transport rate in winter season; the bar area has a strong correlation with wave height.
- (2) In the experiment without spur dikes, the scour depth of the river-mouth channel became large because the flow converges into the channel. On the other hand, in the experiments with the spur dikes, the erosion of the river-mouth bar became active and the scour depth of the river-mouth channel became small because the spur dikes redirected the flow toward the river-mouth bar. Sediments deposited at the lower part of the spur dikes because the flow intensity was weak there.
- (3) The simulation results showed that the bar area and height of the river-mouth bar considerably decrease in the early stage of the flood period, and that the decrease rate after that is relatively small. Over 3,000 m<sup>3</sup>/s of flood discharge accelerates the erosion of the bar, and it also decreases its area remarkably. The mechanisms of flow which takes a long way around the spur dikes and river bed variation process were clarified by the reproduction calculation of the experiments.

## ACKNOWLEDGEMENTS

As for conducting this research, we could obtain the many meteorological and hydrological data from the Fukuchiyama Work Office in Kinki Regional Development Bureau of the Ministry of Land, Infrastructure, Transport and Tourism (MLIT), Japan. Part of this research was financially supported by the Grant-in-Aid for Technical Research Development for River and Erosion-control Engineering from MLIT and the Grant for Joint Research with College of Technologies and the Nagaoka University of Technology. The authors express our gratitude to the related agencies.

## NOTATION

$c_b$	reference concentration of suspended sediment
$d_m$	mean grain diameter
$D_x, D_y$	diffusion term in $x$ and $y$ direction
$g$	gravity acceleration
$h$	water depth
$h_d$	high water level at the Yuragawa River estuary or water surface elevation at downstream end of the channel
$H$	water elevation
$I_b$	sea bed slope behind river-mouth bar in experiments
$L$	length of spur dike
$n$	Manning's roughness coefficient
$q_B$	bed-load sediment transport rate per unit width in streamline direction
$q_{bx}, q_{by}$	bed-load sediment transport rates per unit width
$q_{su}$	release rate of sediment from bed
$Q, Q_p$	water discharge and peak water discharge

$t$	time
$T$	duration time of experiment
$u, v$	velocity components in $x$ and $y$ direction
$w_f$	settling velocity of sediment
$x, y$	plane Cartesian coordinates
$X, Y$	plane coordinates in the channel
$z$	bed elevation
$\lambda$	bed porosity
$\mu_s, \mu_k$	static and kinetic friction coefficient of bed material
$\rho$	fluid density
$\sigma_s$	specific gravity
$\tau_x, \tau_y$	bed shear stress components in $x$ and $y$ direction, and
$\tau^*, \tau^*_c$	dimensionless bed shear stress and dimensionless critical bed shear stress.

## REFERENCES

- Fujita, I., Hara, M., Morimoto, T. and Onishi, T. (1998). Application of PIV techniques to measurement of river surface flows, *Advances in River Engineering*, Vol. 4, JSCE, pp. 41-46,1998.
- International River Interface Corparative (iRIC). (2013). Guide Book on iRIC Seminar in KANSAI, iRIC Project.
- Kanda, K., Miwa, H. and Kato, Y. (2012). Study on dynamic status of river-mouth topography and its control methods in Yuragawa River, Research report on the Grant-in-Aid for Technical Research Development of River and Erosion-control Technology, MLIT.